frontiers | Frontiers in Earth Science

TYPE Original Research
PUBLISHED 28 March 2023
DOI 10.3389/feart.2023.1135512

OPEN ACCESS

EDITED BY
Weiming Liu,
Institute of Mountain Hazards and Environment (CAS), China

REVIEWED BY
Xiangjun Liu,
Jiaying University, China
Jiawei Fan,
Institute of Geology, China Earthquake Administration, China

*CORRESPONDENCE
Fuqiang Li,
lifq@gsau.edu.cn

SPECIALTY SECTION
This article was submitted to Quaternary Science, Geomorphology and Paleoenvironment, a section of the journal Frontiers in Earth Science

RECEIVED 01 January 2023
ACCEPTED 14 March 2023
PUBLISHED 28 March 2023

CITATION
Li F, Pang H and Gao H (2023), Late Pleistocene sedimentary environment reconstruction and evolution in the Houtao Plain.
Front. Earth Sci. 11:1135512.
doi: 10.3389/feart.2023.1135512

Late Pleistocene sedimentary environment reconstruction and evolution in the Houtao Plain

Fuqiang Li[1]*, Hongli Pang[2] and Hongshan Gao[3]

[1]College of Resources and Environmental Sciences, Gansu Agricultural University, Lanzhou, China, [2]Department of Tourism Management, Shanghai Maritime University, Shanghai, China, [3]Key Laboratory of Western China's Environmental Systems (Ministry of Education), College of Earth and Environmental Sciences, Lanzhou University, Lanzhou, China

Reconstructing the Late Pleistocene sedimentary environment history of the Houtao Plain has great significance not only for revealing the evolution of the Yellow River but also for identifying the formation of paleolake and the northern Ulan Buh Desert. This paper presents the results of the sedimentary facies framework based on a grain-size multi-parameter analysis optically stimulated luminescence and ^{14}C dating for a drilling core DKZ06 with a length of 20.04 m from the Houtao Plain. Grain-size multi-parameter analysis was combined with the grain size of modern environmental sediments to the division of the core sedimentary facies in this area. Sedimentary facies of core DKZ06 indicate that the formation of the Houtao Plain area is dominated by fluvial channel deposition and river changed mainly by frequent fluvial channel since ~35 ka. The two episodes of shallow lake deposition from a drilling core, suggesting that there will not be a mega-paleolake in the Houtao Plain, and the frequent channel migration of the Yellow River may have caused a series of furiotile lakes during the Late Pleistocene. The appearance of aeolian sand at the top of core DKZ06 combined with previous stratigraphic records from the adjacent areas indicates that the origin of the northern Ulan Buh Desert is relatively late and it formed only 2,000 years ago. We propose that a combination of river migration and large-scale human activity may be responsible for desert formation. The evolution of sedimentary environments has a close correlation with climate change during the Late Pleistocene. During the interglacial stage (MIS3), the sedimentary environment has a particular lacustrine and fluvial–lacustrine environment because of relatively warm–humid conditions. During the glacial stage (MIS2), the Houtao Plain was dominated by a fluvial sedimentary environment because of a relatively cold and dry climate. The sedimentary environment is complex and changeable during the Holocene (MIS1), which was likely due to the frequent climate fluctuation.

KEYWORDS

grain-size analysis, sedimentary facies, Yellow River, Houtao Plain, drilling core

1 Introduction

The alluvial plain is an important sediment storage unit in fluvial geomorphic systems and also an important settlement for human beings (Wolman and Leopold, 1957; Lambert and Walling, 1987). Alluvial plain deposits are important recorders of the river history and are generally used to infer river responses to external influences (Knox, 2006; Hoffmann et al., 2009; Notebaert and Verstraeten., 2010; Grygar et al., 2011) and also record important information concerning the sedimentary environments for paleoenvironmental

reconstructions, which lies in alluvial plain sediments' spatial ubiquity (Hoffmann et al., 2009). Thus, the identification and reconstruction of paleo-depositional environments provide insights into understanding the spatial and temporal variations of fluvial evolution and regional geomorphic evolution in detail. However, alluvial plain deposits are composed of fine-grained sediments, such as clays, silt, and fine sands (Marriott et al., 1999), and the open-system character of rivers results in the diversity of sedimentary environments in the alluvial plain (Aalto et al., 2003; Hoffmann et al., 2009), which makes sedimentary environment reconstruction more difficult. Thus, grain-size analysis is essential to differentiate sedimentary environments in the alluvial plain (Singh et al., 2007; Kanhaiya et al., 2017).

The Hetao Basin is a key part of the Yellow River drainage basin, and since the current drainage pattern of the Yellow River occurred about 1.2 million years ago (Hu et al., 2017; Wang et al., 2022), the Yellow River's main stream and its tributaries meandered through the basin. The materials carried by fluvial accumulate in the basin to form an alluvial plain, and the sedimentary strata well record the information of the fluvial evolution. Particularly in the western part of the Hetao Basin, numerous paleochannels in the Houtao Plain were formed because of riverbank erosion and sediment deposition caused by extensive river channel migration (Li et al., 2003). In the process of forming the alluvial plain, numerous lakes spread throughout the plain and Ulan Buh Desert, which is adjacent to the Houtao Plain. Previous studies were mainly based on the sedimentary strata investigation of outcrops and drill cores from the Houtao Plain, focusing on the evolution of paleolake and paleo-climate in the Late Pleistocene (Chen et al., 2008; Li et al., 2015; Yang et al., 2018; Cai et al., 2019) and paleoenvironmental evolution of the Ulan Buh Desert (Fan et al., 2010; Zhao et al., 2012; Chen et al., 2014; Li et al., 2014; Li et al., 2015). However, the formation and evolution processes of the paleolake and associated environmental changes of the Ulan Buh Desert have remained elusive. The Yellow River is the main source of water required for the formation of lake environments and supplying sand materials to the Ulan Buh Desert, which is the link between the lake, desert, and other landscapes in this area, so the sedimentary environments of the Houtao Plain are directly connected to the Yellow River evolution. However, little emphasis has been placed in the existing literature on recognizing and explaining how the Yellow River affects the evolution of the paleoenvironment across the plain. The studies on the evolution of this section of the Yellow River are relatively rare. From that mentioned above, it can be seen that exploring the well-dated stratigraphic sequence record of the sedimentary deposits of the Houtao Plain may have important implications not only for reconstructing the evolutionary processes of the Yellow River but also for revealing the paleoenvironmental history of the Houtao Plain.

Within this context, this study aimed to determine the sedimentary facies based on the grain-size characteristics and the occurrence status of sedimentary structures for the drilling core from the Houtao Plain. The grain-size composition and parameters of sediments provide important information on sedimentary processes and sedimentary environments, while grain-size variations of the surficial sedimentary environment in the Houtao Plain are used to interpret the sedimentary facies of the drilling core. In addition, based on detailed sedimentary facies analysis and chronology, this study provides the sedimentary evolution history of the Houtao Plain and then discusses its response to external impacts.

2 Study area

The Houtao Plain is located in the western part of the Hetao Basin and is an important alluvial plain in the Yellow River basin (Figure 1). The Hetao Basin is an EW elongated middle Cenozoic sedimentary basin, which is bounded by the Yinshan Mountains to the north, the Langshan Mountains to the northwest, and the Ordos Plateau to the south. Because the normal faults and buried faults are distributed particularly along the margin of the basin, the Hetao Basin is a fault-defined basin, and within the basin itself develop a series of faults (Research group, 1988). Quaternary deposits in the Hetao Basin comprise dominantly of fluvial–lacustrine facies. The depocenter is located in Linhe subdepression and the maximum sedimentary thickness is over 2400 m since the Quaternary (Yang, 2002). The Yellow River flows into the Hetao Basin; due to the influence of basin subsidence and the continuous accumulation of sediments, the river channel changed from narrow and deep to wider and shallower, and its downstream gradient also becomes smaller, showing a very low gradient (0.15‰); so, the Hetao Basin reaches of the Yellow River are characterized by high-sedimentary loads, severe vertical accretion, and frequent lateral channel migration, forming a typical wide-valley desert and alluvial river channel (Ta et al., 2008; Yao et al., 2011). The Houtao Plain is part of the Hetao Basin, where the fluvial, aeolian, and lacustrine deposits are widely distributed in the plain.

This area is located along the northwestern margin of the East Asian monsoon belt. The mean annual rainfall values are 150–363 mm, and the annual precipitation distribution is uneven, approximately 75% of the annual rainfall is experienced from July to September (Yao et al., 2011). The annual wind speed is about 2.7–4.8 m s^{-1}, with western or northwestern winds predominating in this region, and sandy storms occur more frequently in spring (Pan et al., 2015).

3 Materials and methods

3.1 Drilling and sampling

Sediment core DKZ06 was collected to depths of approximately 20 m at the alluvial plain sites to investigate the stratigraphy of fluvial deposits. We obtained the length of the recovered core as 20.04 m, and the drilling recovery rate for core was > 90%. The drilling core was subsequently split into two halves in the laboratory. One half of each core was used for X-ray fluorescence (XRF) scanning, and the other was divided into 5 cm intervals before describing the specific deposition information, such as composition and structure. The sediments of the drilling core consist mostly of clay, silt, and fine sand. Because the structure of the sediments is disturbed during the drilling process, it could not be observed. Based on the comparative analysis of the grain-size properties of ancient sediments and modern sediments from interrelated sedimentary environments, we conducted particle

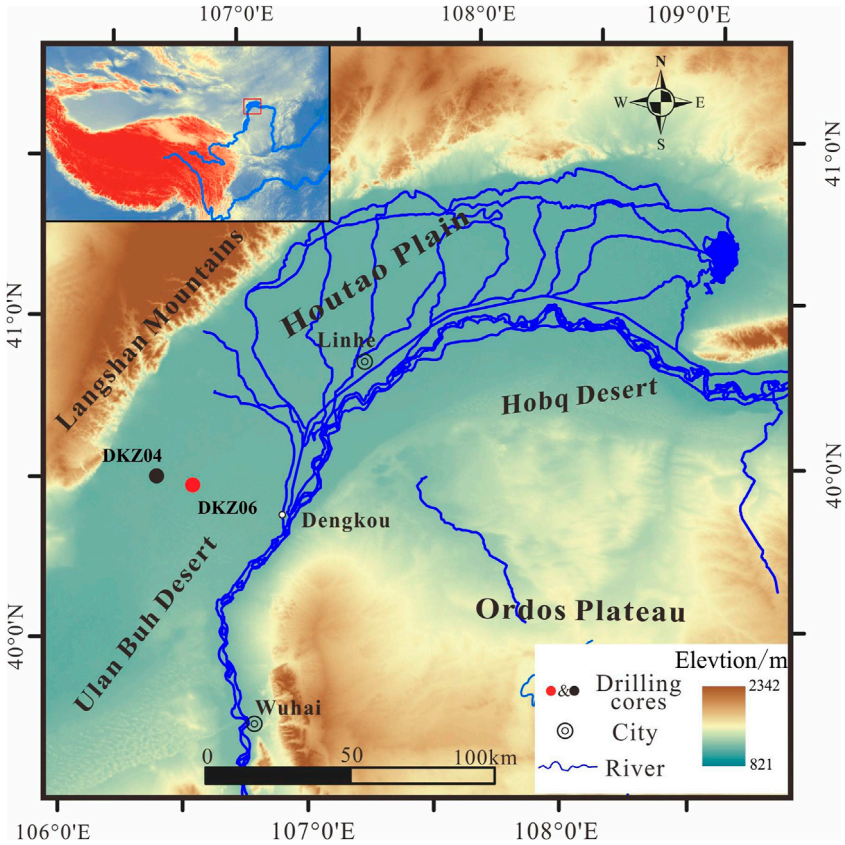

FIGURE 1
Topographic map of the Houtao Plain and its surroundings. The location of the drilling core DKZ06 is shown by a red dot, and the locations of the core DKZ04 (Li et al., 2019) referenced in the text are shown by a black dot. The inset box shows the location of the study area (filled square).

size analysis and correlation through a laser diffraction particle size analyzer in order to present quantitative characteristics of sediments and then reconstruct paleo-depositional environments. Samples were collected at 10 cm intervals for grain-size analysis throughout the core. The results of grain-size analysis of the modern sedimentary environment were reported by Li et al. (2019). Optically stimulated luminescence (OSL) samples were obtained by intercepting a 10 cm length of core before the split, and ^{14}C samples of organic sediments were collected from the clay layer.

The sedimentary sequence of core DKZ06 can be identified as six lithological units (units 1–6) from top to bottom (Figure 2).

Unit 1: 0–1.07 m: This unit mainly consisted of grayish yellow fine sand layers, which is characterized by very low water content, and relatively loose; partial layers of this unit have plant roots.

Unit 2: 1.07–4.07 m: This unit predominantly consisted of brownish yellow and reddish-brown clay. This clay layer was intercalated with several thin layers of grayish-brown silt, and thin horizontal bedding is evident in some clay layers. This unit is characterized by a relatively dense structure and low water content.

Unit 3: 4.07–5.69 m: This unit mainly contained grayish-brown, grayish-green fine sand and medium-coarse sand, without evident horizontal bedding. Some fine-sand and medium-coarse sand layers were intercalated with mud balls and mud lenses.

Unit 4: 5.69–6.7 m. This unit contained brownish-yellow and reddish-brown clay, which were intercalated with several thin layers of grayish-brown silt. This unit is characterized by a relatively dense structure and low water content.

Unit 5: 6.7–19.45 m. This unit mainly consisted of grayish-brown, grayish-green fine sand and medium-coarse sand, without evident horizontal bedding. Some fine-sand and medium-coarse sand layers were intercalated with mud balls and mud lenses.

Unit 6: 19.45–20.04 m. This unit mainly consisted of brownish-yellow and reddish-brown clay, which were intercalated with several thin layers of grayish brown silt. Some clay layers were with conspicuous thin horizontal bedding. This unit is characterized by a relatively dense structure and low water content.

3.2 Grain size

In total, 202 samples from drilling core DKZ06 were selected at 10 cm resolution for particle-size analysis. To examine the longitudinal variation characteristics of sedimentary environment in the drilling core, we collected 164 samples from

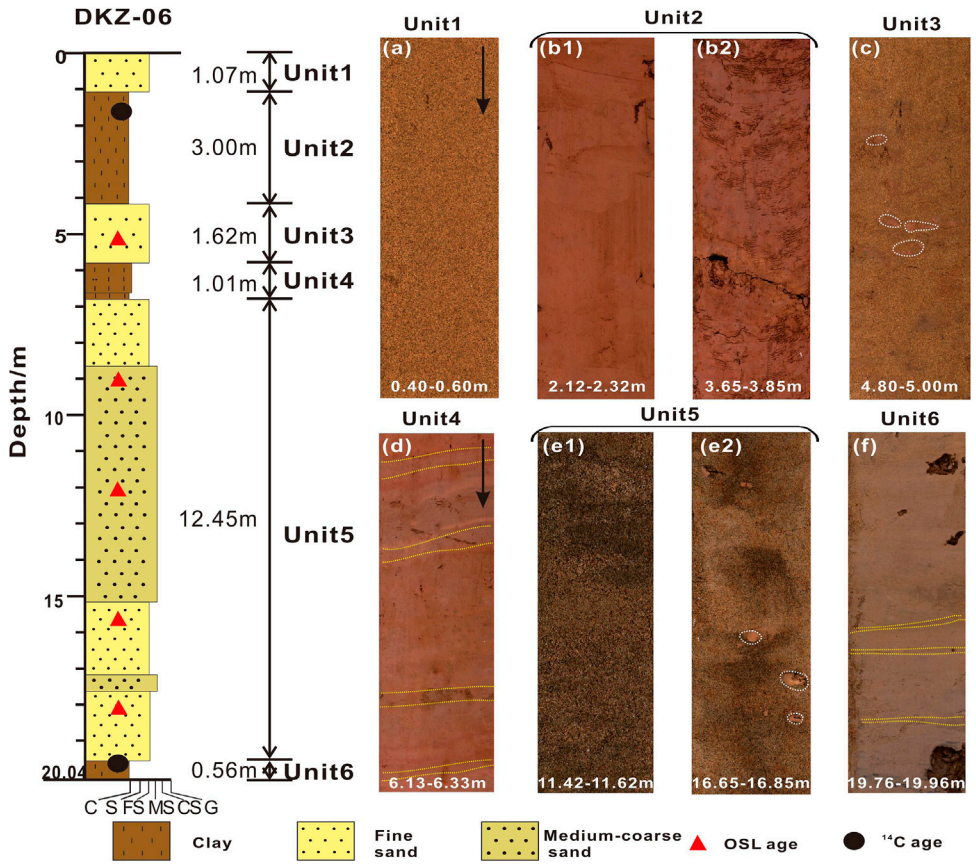

FIGURE 2
Sediment lithology and core photos. **(A)** Fine sand layer in unit 1. **(B1 and B2)** Clay layers in unit 2. **(C)** Fine sand layers intercalated with mud balls and mud lenses (white oval circle) in unit 3. **(D)** Clay layers intercalated with thin silt (yellow line) in unit 4. **(E1 and E2)** Medium-coarse sand and fine-sand layers intercalated with mud balls in unit 5. **(F)** Clay layers intercalated with thin silt (yellow line) in unit 6. The red triangle represents optically stimulated luminescence dating samples; the black dot represents ^{14}C dating samples.

different surface sedimentary environments in the Houtao Plain, including 35 modern fluvial channels, 33 overbank deposition samples along the Inner Mongolian reaches of the Yellow River, 29 surface aeolian sediments from the Ulan Buh Desert, and 69 lacustrine sediments (Li et al., 2019). All samples were treated according to the chemical pre-treatment procedure. First, the samples were treated with 30% H_2O_2 and subsequently 10% HCl, followed by rinsing with distilled water to remove organic materials and carbonate. Second, the samples were mixed with 0.05 mol/L^{-1} $Na(PO_3)_6$ on an ultrasonic vibrator before performing grain-size measurement. Finally, the sub-samples were subjected to grain-size analysis by means of a Malvern 2000 laser grain-size analyzer in the Key Laboratory of Western China's Environmental Systems (Ministry of Education), Lanzhou University. According to the Udden and Wentworth size scales, the grain-size components of sediments are classified as clay (< 3.9 μm), silt (3.9–63 μm), and sand (> 63 μm). All the textural parameters, such as standard deviation (sorting), skewness, kurtosis, mean size, and median particle diameter were calculated according to the percentile statistics from graphical cumulative frequency curves proposed by Folk and Ward (1957).

As one of the most basic characterizations of sediment particles, grain size is closely related to the formation of depositional environment and has been widely used in the sedimentary facies analysis and identification of paleoenvironment (Friedman, 1967; Tanner, 1991; Flemming, 2007; Kanhaiya et al., 2017). The graphical representation of grain-size results, such as frequency distribution curve and cumulative frequency curve, is widely used in the sedimentary facies analysis and paleoenvironment reconstruction because it intuitively and concisely reflects the macroscopic characteristics of a grain-size composition. Furthermore, the various textural parameters plotted on scatter diagrams provided the interpretation of depositional regimes (Tanner, 1991); for example, channel and floodplain deposition samples from the Ganga river can be clearly distinguished through scatter plots of textural parameters (Singh et al., 2007; Kanhaiya et al., 2017). The C–M diagram represents the mode of sediment transportation and provides the dynamic state of sediment transportation, so the transportation and deposition conditions of sediments can be judged. Compared to the projection area of known sedimentary environment samples in the C–M diagram, the origin of unknown sedimentary environment samples can be determined (Passega, 1964; Passega, 1977).

3.3 Chronological dating

Research on the alluvial plain sedimentary process is complicated because of its spatial and temporal complexity, and a series of sample datasets must be analyzed and compared (Hoffmann et al., 2009; Erkens et al., 2011; Grygar et al., 2011). Accurate and precise dating methods and depth–age profiles are clearly essential for establishing a chronological framework of fluvial sedimentation with external forcing factors (Sedláček et al., 2016). OSL dating could provide continuity in a multi-dating method chronology because of the abundance of dating material (quartz and feldspar~) and wide dating timescales (~10 a->100 ka), and it is widely used to date fluvial sediments (Rittenour, 2008; Cunningham and Wallinga, 2012).

Time lines were drawn in the drill cores based on OSL. OSL samples of sand or silt were collected from the core under dark conditions. We collected five OSL samples at different depths of silt and sand layers at core DKZ06. Sample preparation was performed according to the similar procedures described in Lai and Wintle (2006). The unexposed sediments were treated with 10% HCl and 30% H_2O_2 to remove carbonate and organic matters, respectively. Grain-size fractions of 90–125 μm were extracted by wet sieving. The 90–125 μm fractions were treated with 40% HF for about 45 min to remove feldspars and the alpha-irradiated outer layer (10 μm). The extracted quartz grains were washed with 10% HCl to remove fluoride precipitates. Because feldspar contamination can lead to quartz age underestimation, the purity of quartz grains was checked using infrared (830 nm) stimulation, and the results showed that no evident IRSL signals were observed in our samples. The equivalent dose (De) of the quartz extract measurements were made by using an automated Risø TL/OSL-DA-20 reader, and the combination of the single aliquot regenerative (SAR) dose protocol (Murray and Wintle, 2000) and the standard growth curve (SGC) method (Lai et al., 2007), namely, the SAR–SGC method, was used for De determination. Since the partial bleaching of the luminescence signal of river sediments before deposition can lead to overestimation of age, there may be a problem in describing river evolution within the framework of OSL chronology. We used the luminescence signal characteristics of modern fluvial sediments and compared OSL values with radiocarbon ages derived from drilling cores according to previous studies in this area, and the dating results of this method can accurately and precisely estimate the dates of initial sedimentary deposition (Li et al., 2018). In addition to the OSL dating, the two organic materials using ^{14}C dating were found in the drilling core. Radiocarbon dates were calibrated to the calendar year (cal yr BP) using the IntCal13 curve (Reimer et al., 2013) with the calibration performed using the CALIB Rev 7. 0. 0 program (Stuiver and Reimer., 2013).

4 Results

4.1 Grain-size properties of core DKZ06 and sedimentary facies (environments) results

We identified three different sets of facies that represent three different sedimentary environments in the sedimentary sequence of the drilling core based on sediment composition and grain-size characteristics.

Desert: 0–1.07 m (Unit 1). This unit deposits are mainly composed of sand (75%) (Figure 3C; Figure 4A). The grain-size frequency curves illustrate the mode diameters of the sediments are between 200 μm and 300 μm. Mean size values ranged from 133 to 190 μm, with an average value of 171 μm (Figure 3D). The graphical cumulative frequency curves represent fractions transported as the type of multi-saltation and suspension, the cut-off points of saltation fractions and suspension fractions are between 2 and 3Φ, and more than 95% of sediments are saltation fractions (Figure 3G). The grain-size parameters indicate that these sediments are mainly characterized by near-symmetrical and positive skewness and a sharp and narrow distribution of kurtosis curves. In addition, the standard deviation (sorting) of the sediments ranged from 0.5 to 0.9; thus, they are classified as very well sorted (Figure 4B). The grain size C–M patterns indicate that the primary mode of sediment transport is as a rolling component (Figure 4C). The grain size C–M patterns and projections of grain size index features overlap with modern aeolian sand sediments (Figures 4C, D). In conclusion, various grain-size characteristics are similar to those of modern desert environments, so this sequence was interpreted as desert facies deposition.

Fluvial channel: 4.07–5.69 m (unit 3) and 6.7–19.45 m (unit 5): These two unit deposits are mainly composed of sand (more than 60%) (Figure 3C; Figure 4A). The grain-size frequency curves present bimodal and multimodal distribution and show that the mode diameters of the sediments are between 90 μm and 500 μm (Figure 3F). Mean size values ranged from 81 to 404 μm, with an average value of 252.3 μm (Figure 3D). The graphical cumulative frequency curves represent fractions transported as the type of multi-saltation and suspension, and the cut-off points of saltation fractions and suspension fractions are between 1 and 4Φ, and more than 70% of sediments are saltation fractions (Figure 3G). The grain-size parameters indicate that these sediments are mainly characterized by positive skewness and a medium or sharp and narrow distribution of kurtosis curves. In addition, the standard deviation (sorting) of the sediments are widely distributed, ranging from 0.2 to 2.4 (Figure 4B); thus, they are classified as poorly-to-very poorly sorted. The grain size C–M patterns indicate that the primary mode of sediment transport is as a graded suspension with a rolling component (Figure 4C). The grain size C–M patterns and projections of grain size index features overlap with modern aeolian sand sediments (Figures 4C, D). In conclusion, various grain-size characteristics are similar to those of modern fluvial channel sediments, so this sequence was interpreted as desert facies deposition. Furthermore, the presence of mud lenses and balls within the sand (Figures 2C, E) indicates the associated fluvial channel environments (Rust and Nanson, 1989; Maroulis et al., 2007; Nanson et al., 2008).

Lake: 1.07–4.07 m (unit 2), 5.69–6.7 m (unit 4), and 19.45–20.04 m (unit 6): These three unit deposits are mainly composed of silt (40–80%) and clay (20–50%) (Figure 3C; Figure 4A). The grain-size frequency curves present bimodal distribution and show that the mode diameters of the sediments are between 5 μm and 20 μm (Figure 3F). Mean size values ranged from 5 to 45 μm, with an average value of 11.4 μm (Figure 3D). The graphical cumulative frequency curves represent fractions

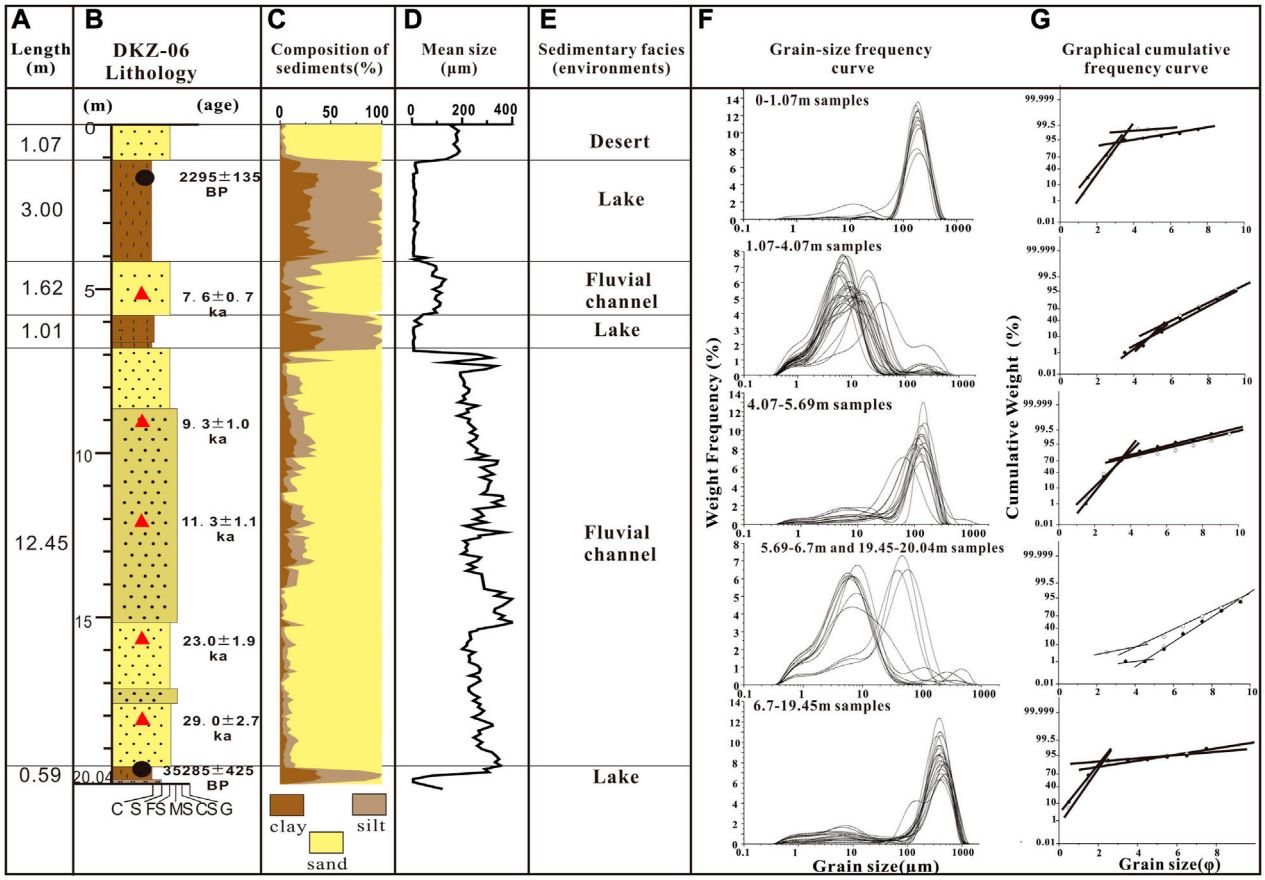

FIGURE 3
Grain-size and classification of sedimentary facies in the drilling core DKZ06. **(A)** Length of each sedimentary facies. **(B)** Lithology of the drilling core DKZ06 and dating results. **(C)** Grain-size composition of drilling core sediments. **(D)** Mean size of drilling core sediments. **(E)** Sedimentary facies based on grain-size characteristics. **(F)** Grain-size frequency curves of core sediments in different units. **(G)** Graphical cumulative frequency curves of core sediments in different units.

transported as the type of saltation and multi-suspension, the cut-off points of saltation fractions and suspension fractions are between 4 and 6Φ, and more than 70% of sediments are suspension fractions (Figure 3G). The grain-size parameters indicate that these sediments are mainly characterized by negative skewness (SK=−0.2–0.2). The kurtosis is 0.8–1.2, revealing that kurtosis curves change from a platykurtic to medium distribution. In addition, the standard deviation (sorting) of the sediments are widely distributed, ranging from 1.2 to 2.2 (Figure 4B); thus, they are classified as poorly-to-very poorly sorted. The grain size C–M patterns indicate that the primary mode of sediment transport is as a uniform suspension component (Figure 4C), which is triggered by continuously decreasing hydrodynamic energy, and represents a lake environment. The grain size C–M patterns and projections of grain-size index features overlap with modern lake sediments (Figures 4C, D). In conclusion, various grain-size characteristics are similar to those of modern lake sediments, so this sequence was interpreted as lacustrine facies deposition.

In summary, based on the characteristic of lithology's visual observation, the analysis of grain-size, and the grain-size distribution of sediments from different surface sedimentary environments in the Houtao Plain, the sediments of core DKZ06 exhibit the characteristics of fluvial–lacustrine deposits. From 4.07 to 5.69 m (unit 3) and 6.7 to 19.45 m (unit 5), the sediments comprised primarily fluvial channel deposits. From 1.07 to 4.07 m (unit 2), 5.69 to 6.7 m (unit 4), and 19.45 to 20.04 m (unit 6), the sediments comprised primarily lacustrine deposits. The uppermost 1.07 m of the core comprised aeolian sand.

4.2 Chronology

OSL and ^{14}C dating were applied to establish the chronology for this drilling core. The De values and OSL apparent ages for the core samples are shown in Table 1, and the ^{14}C dates are shown in Table 2. It is apparent that the OSL ages from core DKZ06 increased with an increasing depth, and the OSL ages are in the correct stratigraphical order and fall within the 29 to 7.6 ka range. Two ^{14}C dates were collected at a depth of 1.5 m and 19.5 m from the drilling core, and the dating results were 2160–2430 cal BP and 34860–35710 cal BP. The ^{14}C ages were categorized into the same stratigraphic order as the OSL ages.

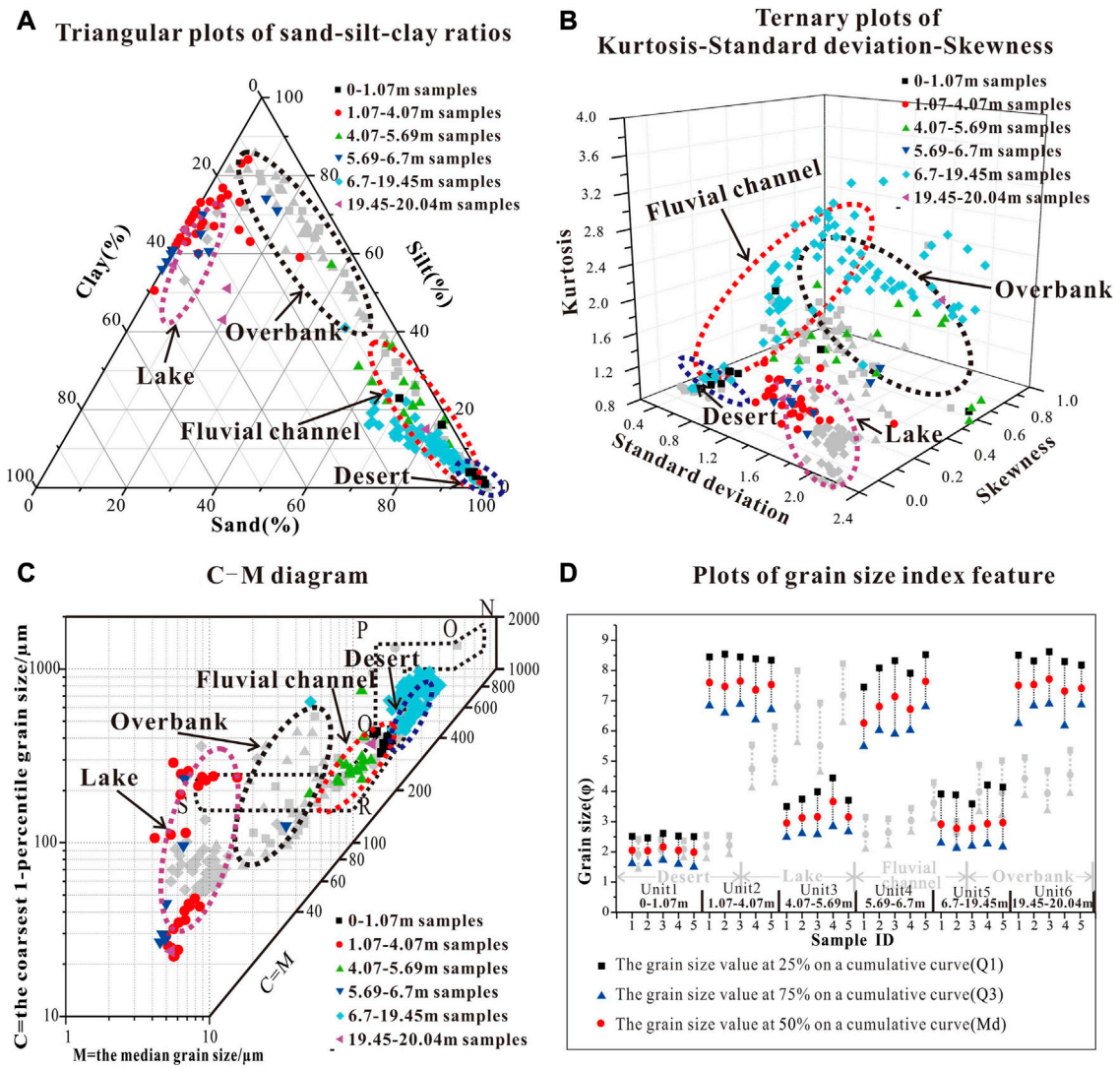

FIGURE 4
(A) Triangular plots of sand–silt–clay ratios in different units. **(B)** Ternary plots of kurtosis–standard deviation–skewness in different units. **(C)** C–M diagram of core sediments. **(D)** Grain-size index feature graphic of core sediments in different units. Gray scatters represent the modern samples from different sedimentary environments (Li et al., 2019). Note that the modern samples from different sedimentary environments occupy different areas.

TABLE 1 Summary of dosimetry and OSL ages at core DKZ06.

Sample ID	Depth (m)	K (%)	Th (ppm)	U (ppm)	Water content (%)	Dose rate (Gy/ka)	De (Gy)	OSL age (a)
DKZ06-07	5.1	1.81 ± 0.07	6.09 ± 0.23	1.30 ± 0.14	8 ± 5	2.59 ± 0.20	19.74 ± 0.84	7.6 ± 0.7
DKZ06-10	9.0	1.59 ± 0.06	3.33 ± 0.18	0.92 ± 0.13	15 ± 5	1.75 ± 0.14	16.28 ± 1.20	9.3 ± 1.0
DKZ06-12	12.0	1.58 ± 0.06	3.65 ± 0.17	0.79 ± 0.13	13 ± 5	1.75 ± 0.14	19.74 ± 1.05	11.3 ± 1.1
DKZ06-15	15.6	1.51 ± 0.06	5.00 ± 0.20	1.09 ± 0.13	19 ± 5	1.83 ± 0.14	41.91 ± 1.30	23.0 ± 1.9
DKZ06-16	18.0	1.62 ± 0.06	3.72 ± 0.19	0.92 ± 0.14	18 ± 5	1.68 ± 0.13	48.71 ± 2.46	29.0 ± 2.7

TABLE 2 Sample data and ^{14}C age results for two samples from core DKZ06.

Sample ID	Depth/m	Material	$\delta^{13}C$ (‰)	^{14}C age BP (a)	Calibrated age 95.4% confidence interval (cal BP)
DKZ06-02	1. 5	Clay	−22.5	2310 ± 40	2160–2430
DKZ06-17	19. 5	Clay	−23.6	31410 ± 170	34860–35710

5 Discussion

5.1 Discriminating between the paleo-depositional environments

Sediment grain-size parameters can provide important information concerning depositional processes and environments because the size-range, mixing, and sorting of sediment populations vary systematically in relation to sedimentary processes, dynamics, and provenance (Doeglas, 1968; Singh et al., 2007; Miall, 2013; Kanhaiya et al., 2017). Thus, the analysis of grain-size composition and textural parameters are the basis for determining the process-response characteristics of individual sediment units and their environment. The grain-size composition and parameters for the investigated 166 samples were evaluated in an attempt to find which parameter or parameter combination can be employed to discriminate between the four major modern depositional environments of the Houtao Plain which were the fluvial channel environment, fluvial overbank environment, lake environment, and desert environment. The most useful graphic grain-size parameters that can be proposed to discriminate between the four depositional environments are correlating graphics of the grain-size composition, such as triangular plots of sand–silt–clay ratios (Figure 4A) and grain-size frequency curves (Figure 3F). The desert and fluvial channel sediments are dominated by sand components, the sediments of the overbank are mainly occupied by silt (more than 50%), and the lake sediments are mainly silt and clay. Interpreting the stratigraphy from drilling cores with no evident structures has proven to be problematic because of the difficulty in differentiating between aeolian and fluvial channel sands (Maroulis et al., 2007). However, texturally, the dunes exhibited unimodal, leptokurtic skewed, and moderately very well sorted fine sand. In contrast, the fluvial channel sediments commonly display a wider range of mean sizes, which are often bimodal and multimodal distribution, coarsely skewed, and very poorly sorted (Figure 4B). Therefore, ternary plots of kurtosis-standard deviation-skewness can be employed successfully to discriminate between the fluvial channel sand deposits and aeolian sand deposits. Although the overbank and lake sediments are dominated by suspended components, they can still be availably distinguished based on the graphic of parameter combination (Figure 4). In addition to the significant differences of particle-size composition, sorting, and parameter combination, the boundaries of point groups are significantly different, even though the particle-size characteristics of different environmental sediments overlap. Furthermore, it is applied to the division of the core sedimentary facies in the area.

5.2 The fluvial evolution and the evolvement of sedimentary environments

For the statistical proportion of each sedimentary facies in the drilling core, the thickness of fluvial channel facies is 4.6 m and it makes up 72% of the drilling core, the lake facies deposits are 4.6 m thick and comprise 23% of the drilling core, and the desert facies is distributed at the top of the core and the thickness is 1.07 m. Sedimentary facies analysis results indicate that the fluvial channel components dominated the strata, suggesting that this area is dominated by fluvial deposition. In particular, fluvial channel sediments were developed with a thickness of 12.65 m from 6.7 m to 19.45 m (Unit 5). The presence of extremely thick sedimentary strata suggested that the river changed due to frequent fluvial channel migration or lateral migration (Rust and Nanson, 1989), and these processes can erode silt and clay from their original floodplain or lacustrine deposits, resulting in the accumulation of multiple channel sediments and representing multiple channel migrations. At this stage, the fine-sand and medium-coarse sand layers were intercalated with mud balls and mud lenses, and this phenomenon indicates that the fine overbank deposition must have been reworked by the laterally active channels (Figure 2E) (Maroulis et al., 2007; Nanson et al., 2008). Alluvial plains of large rivers are built by three modes of river activities, mainly including the lateral point-bar aggradation and the vertical aggradation of sediments carried in diffuse overbank flows and in channelized flows, which are often largely destroyed by channel lateral migration and bank erosion (Dunne et al., 1998). In core DKZ06, more than 70% of fluvial channel sediments accumulated in a normal Houtao Plain environment (Figure 5), which suggests that the shaping process of the plain was dominated by fluvial channel deposition.

The analysis of the sedimentary facies and chronology showed that lakes existed in this area before 35.71 ka, and fluvial channel depositions were followed by two episodes of lake deposition. These units (unit 2, 4, and 6) consisted of mainly brownish-yellow and reddish-brown clay and contained horizontal lamination (Figures 2D, F), which indicated that these strata might be of shallow-water origin and an oxidizing sedimentary environment, and the shallow lake facies are commonly associated with the floodplain sequence (Reading, 2009). With regard to the formation of a lake environment, some authors suggest that a mega-paleolake once existed in the Hetao Basin during the Late Pleistocene in the case of the raised outlet of the basin and increased in surface runoff (Chen et al., 2008; Jia et al., 2016; Li et al., 2017; Yang et al., 2018). However, combining with another drilling core DKZ04, a lacustrine clay unit occurs at the bottom of the core, and the sedimentary facies are dominated by fluvial channel and overbank deposition (Figure 5) (Li et al., 2019). The thickness and discontinuity of the lake sedimentary facies indicated that there will not be a mega-paleolake, which suggests that the lake formed directly during channel migration, and it is a type

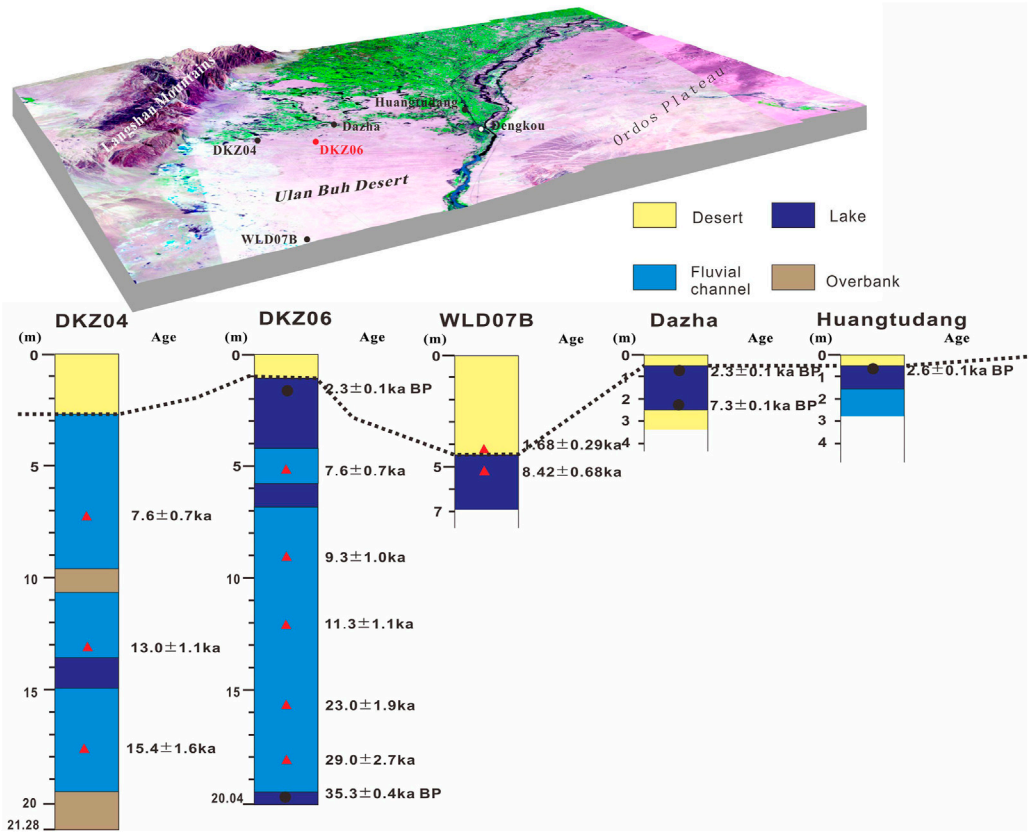

FIGURE 5
Sedimentary facies correlation of three drill cores and two sections in the Houtao Plain. The OSL and ^{14}C dating results of cores DKZ04, DKZ06, WLD07B, and sections Dazha, Huangtudang. Dashed lines show the correlation of the bottom of the desert sediment. The sedimentary facies and OSL ages of WLD07B are from Fan et al. (2010), and sedimentary facies and ^{14}C ages of sections Dazha, Huangtudang are from Jia and Yin (2004).

of furiotile lake. The lake is controlled by the amount of the Yellow River's water, during the flood period, when sufficient water was ponded into a lake, and a series of furiotile lakes joined together to form a large lake. However, the lake began to gradually recede and run dry because the fluvial channel is diverted away from the lake. Similarly, the northern part of the plain is now dotted with numerous lakes. It may have formed due to the Yellow River's main current that moved from north to south of the Houtao Plain and, perhaps, were proto-river channels (Wu et al., 2013).

The presence of aeolian sand in strata is the most direct and reliable evidence of the emergence and expansion of deserts (Dong et al., 1983). The desert facies appeared only at the top of drilling cores DKZ06 and DKZ04, A^{14}C age of 2295 ± 135 cal BP was obtained from the clay layer at the top 1.5 m of the core DKZ06, and the clay layer was covered with aeolian sand, so it can be inferred that the aeolian sand accumulation occurred after 2.3 ka (Figure 5). In addition, in the DKZ04 core, based on the rate of sedimentation, it is calculated that the age of aeolian sand deposition in this area occurred after 2.6 ka (Li et al., 2019). This evidence suggested that the northern Ulan Buh Desert was formed in the late Holocene, at least since ~2 ka. Hou and Yu (1973) suggested that the northern Ulan Buh Desert was formed after the Han dynasty based on a detailed field survey of archaeological sites and historical documents. Chronological work on aeolian sand overlaying lacustrine layers suggested that the modern desert landscape of the northern Ulan Buh Desert was formed before the Han dynasty (Figure 5) (Jia and Yin, 2004). Fan et al. (2010) dated an aeolian sand sequence in the interior Ulan Buh Desert using quartz OSL dating and concluded the northern Ulan Buh Desert formed gradually at least~2 ka (Figure 5). These observations are consistent with our interpretation that the aeolian sand dunes formed in the northern Ulan Buh Desert since ~2 ka.

Oxygen isotopic records of stalagmites from the Dongge cave showed that the East Asian summer monsoon was strong during 2.2–1.7 ka (Wang et al., 2005). Meanwhile, other climatological data from the region and around also showed that the effective humidity in the study area was relatively high during this period (Fan et al., 2013). Such a climatic condition does not promote large amounts of sand supply. Thus, all of this evidence suggests that it is difficult to interpret the rapid sand accumulation covering large areas that has occurred based on climate change during 2 ka. It is apparent that aeolian sand is formed directly on channel sands and furiotile lake clays based on the chronology and stratigraphy of drilling cores DKZ04 and DKZ06 (Figure 5) and formed at least by ~2 ka, as a result of river channel migration. Historical documents displayed that the main channel of the Yellow River flows in front of the Langshan Mountains before 2 ka, a large number of lakes developed in front of the mountains subsequently, the diversion and abandonment of the Yellow River led to the drying up of lakes and desertification of oases (Li et al., 2003), and the channel lateral migration and bank erosion provided the

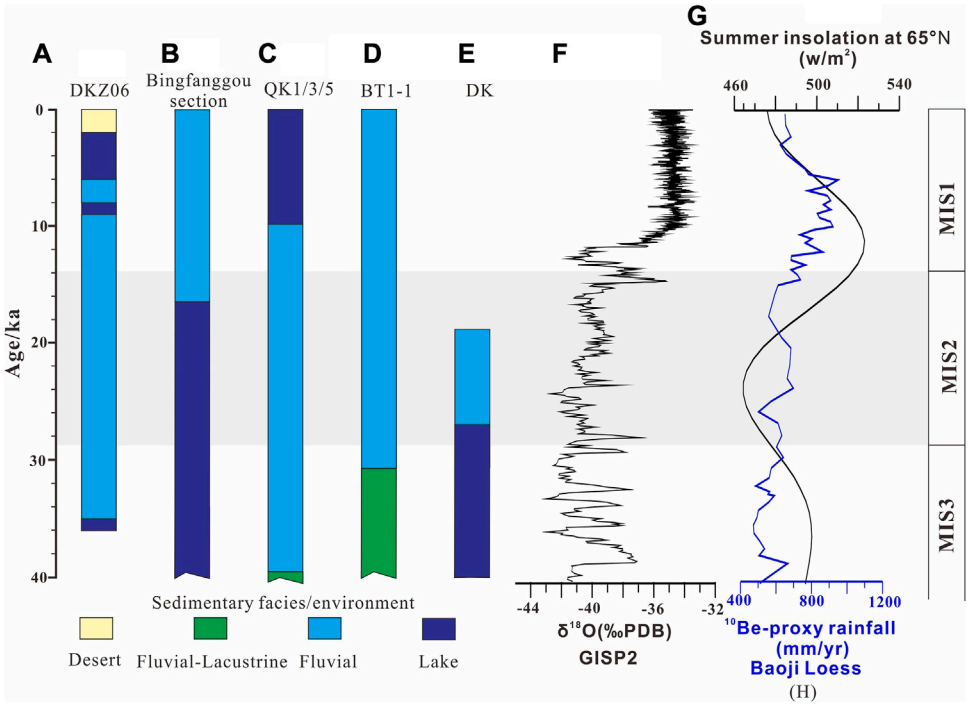

FIGURE 6
Relationships between the sedimentary environment and climate change during the Late Pleistocene. **(A)** Sedimentary facies of core DKZ06. **(B)** Sedimentary facies of the Bingfanggou section (Yang et al., 2018). **(C)** Sedimentary facies of cores QK1, QK3, and QK5 (Liu et al., 2014). **(D)** Sedimentary facies of core BT1-1 (Zhao et al., 2016). **(E)** Sedimentary facies of core DK (Yang et al., 2020). **(F)** $\delta^{18}O$ record of GISP2 (Stuiver and Grootes, 2000). **(G)** Plot of 65°N summer insolation (Berger and Loutre, 1991). **(H)** ^{10}Be-proxy rainfall of Baoji Loess (Beck et al., 2018)

material basis for the formation of the desert. In addition, humans exert a definitive impact upon the environment with the increase in population, when they alter terrestrial vegetation patterns during the rapid development of agriculture, and when a dramatic increase in population necessitates major changes in land use (Vitousek et al., 1997). Historic records revealed that the period of land desertification corresponded to the Qin and Han dynasties of large-scale immigration (Wang, 1991). With the rapid increase of population and the enhancement of agricultural activities, the harmonious natural environment of the Hetao Plain had been destroyed. Extensive deforestation and grasslands reclamation in this area occurred on a large scale, as a result of immigration, cultivation, and military occupation, leading to artificial agricultural vegetation continuously replacing the natural vegetation of forests and grasses and also increasing the risk of fluvial sediments erosion by rain or wind. Subsequently, farmland abandoned owing to poor land management had intensified the process of desertification during the end of the Han dynasty (~200 AD) (Hou, 1973). This showed that the present desert landscape started to develop rapidly in the northern Ulan Buh Desert area at around 2 ka, triggered both by the migration of the river and by the large scale human activity.

The sedimentary facies and chronology in the drilling core indicates that the sedimentary environment comprised mainly fluvial–lacustrine deposits during ~35 ka. In addition, the records of the sedimentary environment from sedimentary sections and drilling cores on the Houtao Plain also suggested that the area probably consisted of fluvial–lacustrine systems during the Late Pleistocene (Liu et al., 2014; Zhao et al., 2016; Yang et al., 2018; Yang et al., 2020) (Figure 6). However, these dates show that the inconsistency of regional sedimentary environmental development and the inconsistency in sedimentary environments may have been the results of the Yellow River's frequent lateral migration and inflow condition. Therefore, climate may be the dominant factor of regional environmental evolution, and regional climate change is consistent with other East Asian monsoon regions (Cai et al., 2019). Affected by the decrease of solar radiation in the Northern Hemisphere and the increase of global ice volume, the climate has experienced several changes from cold and dry, warm, and humid alternations to drought since the last glacial period (Figure 6). The late glacial stage (MIS2) of the last glacial period is relatively cold and dry, and the interglacial stage (MIS3) is warm and dry. During the Holocene (MIS1), the overall climate is relatively warm and humid, but the climate fluctuations are more frequent. During the interglacial stage (MIS3), the sedimentary environment comprised mainly lacustrine and fluvial–lacustrine environments, and the amount of water in the Houtao Plain reach increases because of relatively warm–humid conditions. During the glacial stage (MIS2), relatively cold and dry climatic conditions control inflow reduction, so it is dominated by the fluvial sedimentary environment. The sedimentary environment is complex and changeable during the Holocene (MIS1), which is likely linked to the frequent climate fluctuation, and the development of lacustrine environment may have been responsive to the warm and humid climate.

6 Conclusion

Environmental proxy indexes of grain-size analysis and reliable quartz OSL and ^{14}C dating ages were employed to interpret the sedimentary environment sequence represented in the drilling core DKZ06 from the Houtao Plain, the western Hetao Basin. The results showed that the core sediments could be effectively identified using a combination of the grain size multi-parameters analysis and the grain size of modern environmental sediments in this area, and it had potential to be an effective method when it is difficult to differentiate sedimentary stratigraphy elsewhere. The temporal and spatial distribution of the sedimentary facies from the drilling core showed that the sedimentary environment and the shaping processes of the plain were dominated by fluvial channel deposition. The thickness and discontinuity of the lake sedimentary facies suggested that there would not be a mega-paleolake in the Houtao Plain, and the frequent channel migration of Yellow River may have caused a series of furiotile lakes during the Late Pleistocene. In combination with the stratigraphic records from other drilling cores and sections in the adjacent areas, the results revealed aeolian sand dunes formed in the northern Ulan Buh Desert since ~2 ka. A combination of the river migration and the large-scale human activity may be responsible for the formation of desert landscapes in the northern Ulan Buh Desert. These results suggested that the fluvial channel migration of the Yellow River would have not only made an important contribution to the paleolake formation and demise but would have also been an important reason for the formation of sand dunes in the plain. The evolution of sedimentary environments inferred from cores has a close correlation with climate change during the Late Pleistocene. During cold phases, the Houtao Plain was dominated by the fluvial sedimentary environment. During warm phases, the sedimentary environment was characterized by lacustrine and fluvial–lacustrine environments.

Data availability statement

The original contributions presented in the study are included in the article/Supplementary Material; further inquiries can be directed to the corresponding author.

Author contributions

FL wrote the first draft of the manuscript and conducted the field and lab work with the help of HP, and HG contributed to conception and design of the study and led the field investigations. All authors participated in the discussion and modification and approved the submitted version.

Funding

This research was supported by the National Natural Science Foundation of China (Grant No. 42001008; 42001004; and 42171002) and scientific research start-up funds for openly recruited doctors (GAU-KYQD-2019-11).

Acknowledgments

The authors would like to thank Lianke Zhang, Zongmeng Li, Fengliang Liu, and Xiaopeng Liu for their fieldwork assistance, and Yixuan Wang and Xiaoyun Yang (Qinghai Institute of Salt Lakes, Chinese Academy of Sciences) are acknowledged for their work on OSL dating measurements.

Conflict of interest

The authors declare that the research was conducted in the absence of any commercial or financial relationships that could be construed as a potential conflict of interest.

Publisher's note

References

Aalto, R., Maurice-Bourgoin, L., Dunne, T., Montgomery, D. R., Nittrouer, C. A., and Guyot, J. L. (2003). Episodic sediment accumulation on Amazonian flood plains influenced by El Nino/Southern Oscillation. *Nature* 425 (6957), 493–497. doi:10.1038/nature02002

Cai, M., Ye, P., Yang, X., and Li, C. (2019). Vegetation and climate change in the Hetao Basin (Northern China) during the last interglacial-glacial cycle. *J. Asian Earth Sci.* 171, 1–8. doi:10.1016/j.jseaes.2018.11.024

Chen, F., Fan, Y., Chun, X., Madsen, D. B., Oviatt, C. G., Zhao, H., et al. (2008). Preliminary research on megalake jilantai-hetao in the arid areas of China during the late quaternary. *Chin. Sci. Bull.* 53 (11), 1725–1739. doi:10.1007/s11434-008-0227-3

Chen, F., Li, G., Zhao, H., Jin, M., Chen, X., Fan, Y., et al. (2014). Landscape evolution of the ulan Buh Desert in northern China during the late quaternary. *Quat. Res.* 81 (3), 476–487. doi:10.1016/j.yqres.2013.08.005

Cunningham, A. C., and Wallinga, J. (2012). Realizing the potential of fluvial archives using robust OSL chronologies. *Quat. Geochronol.* 12, 98–106. doi:10.1016/j.quageo.2012.05.007

Doeglas, D. J. (1968). Grain-size indices, classification and environment. *Sedimentology* 10 (2), 83–100. doi:10.1111/j.1365-3091.1968.tb01101.x

Dong, G. R., Li, B. S., and Gao, S. Y. (1983). Significance of quaternary paleoaeolian sand found in Ordos Plateau. *Chin. Sci. Bull.* 16, 998–1001. (in Chinese).

Dunne, T., Mertes, L. A., Meade, R. H., Richey, J. E., and Forsberg, B. R. (1998). Exchanges of sediment between the flood plain and channel of the Amazon River in Brazil. *Geol. Soc. Am. Bull.* 110 (4), 450–467. doi:10.1130/0016-7606(1998)110<0450:EOSBTF>2.3.CO;2

Erkens, G., Hoffmann, T., Gerlach, R., and Klostermann, J. (2011). Complex fluvial response to lateglacial and Holocene allogenic forcing in the lower rhine valley (Germany). *Quat. Sci. Rev.* 30 (5-6), 611–627. doi:10.1016/j.quascirev.2010.11.019

Fan, Y., Chen, F., Fan, T., Zhao, H., and Yang, L. (2010). Sedimentary documents and Optically Stimulated Luminescence (OSL) dating for formation of the present landform of the northern Ulan Buh Desert, northern China. *Sci. China Earth Sci.* 53 (11), 1675–1682. doi:10.1007/s11430-010-3085-1

Fan, Y., Chen, X., Fan, T., Jin, M., Liu, J., and Chen, F. (2013). Sedimentary and OSL dating evidence for the development of the present Hobq desert landscape, northern China. *Sci. China Earth Sci.* 56 (12), 2037–2044. doi:10.1007/s11430-013-4673-7

Flemming, B. W. (2007). The influence of grain-size analysis methods and sediment mixing on curve shapes and textural parameters: Implications for sediment trend analysis. *Sediment. Geol.* 202 (3), 425–435. doi:10.1016/j.sedgeo.2007.03.018

Folk, R. L., and Ward, W. C. (1957). Brazos River bar [Texas]; a study in the significance of grain size parameters. *J. Sediment. Res.* 27 (1), 3–26. doi:10.1306/74D70646-2B21-11D7-8648000102C1865D

Friedman, G. M. (1967). Dynamic processes and statistical parameters compared for size frequency distribution of beach and river sands. *J. Sediment. Res.* 37 (2), 327–354. doi:10.1306/74D716CC-2B21-11D7-8648000102C1865D

Grygar, T. M., Nováková, T., Mihaljevič, M., Strnad, L., Světlík, I., Koptíková, L., et al. (2011). Surprisingly small increase of the sedimentation rate in the floodplain of Morava River in the Strážnice area, Czech Republic, in the last 1300 years. *Catena* 86 (3), 192–207. doi:10.1016/j.catena.2011.04.003

Hoffmann, T., Erkens, G., Gerlach, R., Klostermann, J., and Lang, A. (2009). Trends and controls of Holocene floodplain sedimentation in the Rhine catchment. *Catena* 77 (2), 96–106. doi:10.1016/j.catena.2008.09.002

Hou, R. (1973). Archaeological discovery and changes of geographical environment in Ulan Buh Desert. *Archaeology* 2, 92–107. (in Chinese). doi:10.13619/j.cnki.cn11-1532/k.1973.01.006

Hu, Z., Pan, B., Bridgland, D., Vandenberghe, J., Guo, L., Fan, Y., et al. (2017). The linking of the upper-middle and lower reaches of the Yellow River as a result of fluvial entrenchment. *Quat. Sci. Rev.* 166, 324–338. doi:10.1016/j.quascirev.2017.02.026

Jia, L., Zhang, X., Ye, P., Zhao, X., He, Z., He, X., et al. (2016). Development of the alluvial and lacustrine terraces on the northern margin of the Hetao Basin, inner Mongolia, China: Implications for the evolution of the Yellow River in the Hetao area since the late pleistocene. *Geomorphology* 263, 87–98. doi:10.1016/j.geomorph.2016.03.034

Jia, T. F., and Yin, S. (2004). Geomorphic evolution in northern ulan Buh Desert in the Holocene. *Sci. Geogr. Sin.* 24, 217–221. (in Chinese). doi:10.3969/j.issn.1000-0690.2004.02.015

Kanhaiya, S., Singh, B. P., Tripathi, M., Sahu, S., and Tiwari, V. (2017). Lithofacies and particle-size characteristics of late Quaternary floodplain deposits along the middle reaches of the Ganga river, central Ganga plain, India. *Geomorphology* 284, 220–228. doi:10.1016/j.geomorph.2016.08.030

Knox, J. C. (2006). Floodplain sedimentation in the upper Mississippi valley: Natural versus human accelerated. *Geomorphology* 79 (3-4), 286–310. doi:10.1016/j.geomorph.2006.06.031

Lai, Z. P., Brückner, H., Zöller, L., and Fülling, A. (2007). Existence of a common growth curve for silt-sized quartz OSL of loess from different continents. *Radiat. Meas.* 42 (9), 1432–1440. doi:10.1016/j.radmeas.2007.08.006

Lai, Z. P., and Wintle, A. G. (2006). Locating the boundary between the Pleistocene and the Holocene in Chinese loess using luminescence. *Holocene* 16 (6), 893–899. doi:10.1191/0959683606hol980rr

Lambert, C. P., and Walling, D. E. (1987). Floodplain sedimentation: A preliminary investigation of contemporary deposition within the lower reaches of the river culm, devon, UK. *Geogr. Ann. Ser. A, Phys. Geogr.* 69 (3-4), 393–404. doi:10.1080/04353676.1987.11880227

Li, B., Ge, Q., and Zheng, J. Y. (2003). Evolution of the Yellow River in the Houtao Plain of inner Mongolia in the past 2000 years. *Acta Geogr. Sin.* 2, 239–246. (in Chinese). doi:10.11821/xb200302011

Li, B., Sun, D., Xu, W., Wang, F., Liang, B., Ma, Z., et al. (2017). Paleomagnetic chronology and paleoenvironmental records from drill cores from the Hetao Basin and their implications for the formation of the Hobq Desert and the Yellow River. *Quat. Sci. Rev.* 156, 69–89. doi:10.1016/j.quascirev.2016.11.023

Li, F., Pan, B., Lai, Z., Gao, H., and Ou, X. (2018). Identifying the degree of luminescence signal bleaching in fluvial sediments from the Inner Mongolian reaches of the Yellow River. *Geochronometria* 45 (1), 82–96. doi:10.1515/geochr-2015-0087

Li, F. Q., Gao, H. S., Zhang, L. K., Li, Z. M., and Pang, H. L. (2019). Grain size characteristics and evolution of core sedimentary environment in the Houtao plain reach of the Yellow river. *Acta Sedimentol. Sin.* 37 (6), 1234–1243. (in Chinese).

Li, G., Jin, M., Chen, X., Wen, L., Zhang, J., Madsen, D., et al. (2015). Environmental changes in the Ulan Buh Desert, southern Inner Mongolia, China since the middle Pleistocene based on sedimentology, chronology and proxy indexes. *Quat. Sci. Rev.* 128, 69–80. doi:10.1016/j.quascirev.2015.09.010

Li, G. Q., Jin, M., Wen, L. J., Zhao, H., Madsen, D., Liu, X. K., et al. (2014). Quartz and K-feldspar optical dating chronology of eolian sand and lacustrine sequence from the southern ulan Buh Desert, NW China: Implications for reconstructing late pleistocene environmental evolution. *Palaeogeogr. Palaeoclimatol. Palaeoecol.* 393, 111–121. doi:10.1016/j.palaeo.2013.11.003

Liu, Z., Zhao, H., Wang, C. M., Ji, Y. P., and Zhang, Y. L. (2014). OSL ages of sedimentary layers in Linhe depression since late pleistocene. *Arid. Land Geogr.* 37 (3), 439–446. (in Chinese). doi:10.13826/j.cnki.cn65-1103/x.2014.03.004

Maroulis, J. C., Nanson, G. C., Price, D. M., and Pietsch, T. (2007). Aeolian–fluvial interaction and climate change: Source-bordering dune development over the past~100 ka on cooper creek, central Australia. *Quat. Sci. Rev.* 26 (3-4), 386–404. doi:10.1016/j.quascirev.2006.08.010

Marriott, S. B., Alexander, J., and Hey, R. (1999). *Floodplains: Interdisciplinary approaches*. London: Geological Society of London.

Miall, A. D. (2013). *The geology of fluvial deposits: Sedimentary facies, basin analysis, and petroleum geology*. Berlin, Heidelberg: Springer.

Murray, A. S., and Wintle, A. G. (2000). Luminescence dating of quartz using an improved single-aliquot regenerative-dose protocol. *Radiat. Meas.* 32 (1), 57–73. doi:10.1016/S1350-4487(99)00253-X

Nanson, G. C., Price, D. M., Jones, B. G., Maroulis, J. C., Coleman, M., Bowman, H., et al. (2008). Alluvial evidence for major climate and flow regime changes during the middle and late Quaternary in eastern central Australia. *Geomorphology* 101 (1-2), 109–129. doi:10.1016/j.geomorph.2008.05.032

Notebaert, B., and Verstraeten, G. (2010). Sensitivity of west and central European river systems to environmental changes during the Holocene: A review. *Earth-Science Rev.* 103 (3-4), 163–182. doi:10.1016/j.earscirev.2010.09.009

Pan, B., Pang, H., Zhang, D., Guan, Q., Wang, L., Li, F., et al. (2015). Sediment grain-size characteristics and its source implication in the Ningxia–Inner Mongolia sections on the upper reaches of the Yellow River. *Geomorphology* 246, 255–262. doi:10.1016/j.geomorph.2015.06.028

Passega, R. (1964). Grain size representation by CM patterns as a geologic tool. *J. Sediment. Petrol.* 34, 830–847. doi:10.1306/74d711a4-2b21-11d7-8648000102c1865d

Passega, R. (1977). Significance of CM diagrams of sediments deposited by suspensions. *Sedimentology* 24 (5), 723–733. doi:10.1111/j.1365-3091.1977.tb00267.x

Reading, H. G. (2009). *Sedimentary environments: Processes, facies and stratigraphy*. Hoboken, New Jersey, U.S.: John Wiley and Sons.

Reimer, P. J., Bard, E., Bayliss, A., Beck, J. W., Blackwell, P. G., Ramsey, C. B., et al. (2013). IntCal13 and Marine13 radiocarbon age calibration curves 0–50,000 years cal BP. *Radiocarbon* 55 (4), 1869–1887. doi:10.2458/azu_js_rc.55.16947

Research group (1988). Of active fault system around the Ordos Massif. *Active Fault system around Ordos massif*. Beijing: Seismology Press. (in Chinese).

Rittenour, T. M. (2008). Luminescence dating of fluvial deposits: Applications to geomorphic, palaeoseismic and archaeological research. *Boreas* 37 (4), 613–635. doi:10.1111/j.1502-3885.2008.00056.x

Rust, B. R., and Nanson, G. C. (1989). Bedload transport of mud as pedogenic aggregates in modern and ancient rivers. *Sedimentology* 36 (2), 291–306. doi:10.1111/j.1365-3091.1989.tb00608.x

Sedláček, J., Bábek, O., and Kielar, O. (2016). Sediment accumulation rates and high-resolution stratigraphy of recent fluvial suspension deposits in various fluvial settings, Morava River catchment area, Czech Republic. *Geomorphology* 254, 73–87. doi:10.1016/j.geomorph.2015.11.011

Singh, M., Singh, I. B., and Müller, G. (2007). Sediment characteristics and transportation dynamics of the Ganga River. *Geomorphology* 86 (1-2), 144–175. doi:10.1016/j.geomorph.2006.08.011

Stuiver, M., and Reimer, P. J. (2013). Radiocarbon calibration program Calib Rev7.0.0. Available at: https://serc.carleton.edu/36729.

Ta, W., Xiao, H., and Dong, Z. (2008). Long-term morphodynamic changes of a desert reach of the Yellow River following upstream large reservoirs' operation. *Geomorphology* 97 (3-4), 249–259. doi:10.1016/j.geomorph.2007.08.008

Tanner, W. F. (1991). *Suite statistics: The hydrodynamic evolution of the sediment pool.Principles, methods and applications of particle size analysis*. Cambridge: University Press, 225–236.

Vitousek, P. M., Mooney, H. A., Lubchenco, J., and Melillo, J. M. (1997). Human domination of Earth's ecosystems. *Science* 277 (5325), 494–499. doi:10.1126/science.277.5325.494

Wang, B. C. (1991). Historical geography study of the hobq desert. *J. Desert Res.* 11 (4), 33. (in Chinese). doi:10.3321/j.issn:1000-694X.1991.04.009

Wang, X., Hu, G., Saito, Y., Ni, G., Hu, H., Yu, Z., et al. (2022). Did the modern yellow river form at the mid-pleistocene transition? *Sci. Bull.* 67, 1603–1610. doi:10.1016/j.scib.2022.06.003

Wang, Y., Cheng, H., Edwards, R. L., He, Y., Kong, X., An, Z., et al. (2005). The Holocene asian monsoon: Links to solar changes and north atlantic climate. *Science* 308 (5723), 854–857. doi:10.1126/science.1106296

Wolman, M. G., and Leopold, L. B. (1957). River flood plains: Some observations on their formation. *Geol. Surv. Prof. Pap.* 2, 87–109. doi:10.3133/pp282C

Wu, J., Ma, L., Yu, H., Zeng, H., Liu, W., and Abuduwaili, J. (2013). Sediment geochemical records of environmental change in lake wuliangsu, Yellow River Basin, north China. *J. Paleolimnol.* 50 (2), 245–255. doi:10.1007/s10933-013-9718-6

Yang, G. (2002). *Identifying sediment sources and their controls in the inner Mongolian reach of the Yellow River*. Beijing: Haiyang Publishing House. (in Chinese).

Yang, X., Cai, M., Hu, J., Ye, P., Ji, F., Zhigao, Z., et al. (2020). The paleolake hydrology and climate change since the~ 40 ka in the Hetao Basin, Inner Mongolia, China. *Quat. Int.* 553, 73–82. doi:10.1016/j.quaint.2020.06.040

Yang, X., Cai, M., Ye, P., Yang, Y., Wu, Z., Zhou, Q., et al. (2018). Late Pleistocene paleolake evolution in the Hetao basin, inner Mongolia, China. *Quat. Int.* 464, 386–395. doi:10.1016/j.quaint.2017.11.047

Yao, Z., Ta, W., Jia, X., and Xiao, J. (2011). bank erosion and accretion along the ningxia–inner Mongolia reaches of the Yellow River from 1958 to 2008. *Geomorphology* 127 (1-2), 99–106. doi:10.1016/j.geomorph.2010.12.010

Zhao, H,M., Zhao, H., Liu, L. J., Zhang, Y. L., and Wang, C. M. (2016). Stratigraphy and environmental evolution of late Quaternary in Baotou area, Inner Mongolia, China. *J. Arid Land Resour. Environ.* 30 (04), 165–171. (in Chinese). doi:10.13448/j.cnki.Jalre.2016.131

Zhao, H., Li, G., Sheng, Y., Jin, M., and Chen, F. (2012). Early–middle Holocene lake-desert evolution in northern ulan Buh Desert, China. *Palaeogeogr. Palaeoclimatol. Palaeoecol.* 331, 31–38. doi:10.1016/j.palaeo.2012.02.027